Field-based simulation of a demonstration site for carbon dioxide sequestration in low-permeability saline aquifers in the Ordos Basin, China

Jian Xie · Keni Zhang · Litang Hu · Paul Pavelic · Yongsheng Wang · Maoshan Chen

Abstract Saline formations are considered to be candidates for carbon sequestration due to their great depths, large storage volumes, and widespread occurrence. However, injecting carbon dioxide into low-permeability reservoirs is challenging. An active demonstration project for carbon dioxide sequestration in the Ordos Basin, China, began in 2010. The site is characterized by a deep, multi-layered saline reservoir with permeability mostly below 1.0×10^{-14} m^2. Field observations so far suggest that only small-to-moderate pressure buildup has taken place due to injection. The Triassic Liujiagou sandstone at the top of the reservoir has surprisingly high injectivity and accepts approximately 80 % of the injected mass at the site. Based on these key observations, a three-dimensional numerical model was developed and applied, to predict the plume dynamics and pressure propagation, and in the assessment of storage safety. The model is assembled with the most recent data and the simulations are calibrated to the latest available observations. The model explains most of the observed phenomena at the site. With the current operation scheme, the CO$_2$ plume at the uppermost reservoir would reach a lateral distance of 658 m by the end of the project in 2015, and approximately 1,000 m after 100 years since injection. The resulting pressure buildup in the reservoir was below 5 MPa, far below the threshold to cause fracturing of the sealing cap (around 33 MPa).

Keywords China · Geological CO$_2$ storage · Multiphase flow · Saline aquifer · TOUGH2

J. Xie · K. Zhang (✉) · L. Hu
College of Water Sciences,
Beijing Normal University, Beijing, 100875, China
e-mail: keniz@bnu.edu.cn

P. Pavelic
International Water Management Institute, Vientiane, Laos PDR

Y. Wang · M. Chen
China Shenhua Coal Liquefaction Co. Ltd. (CSCLC) Ordos, Ordos, 017209, China

Introduction

Carbon dioxide capture and storage (CCS) is presently seen as a viable mitigation strategy for reduction of greenhouse-gas emission into the atmosphere (Bachu 2002; Houghton et al. 1996; IPCC 2005; Ledley et al. 1999). Deep saline aquifers attract the attention of many researchers, due to their greater storage capacity than those of other geological storage options such as depleted oil and gas reservoirs (Eccles et al. 2009; IPCC 2005; US DOE 2007). Pioneering geological carbon dioxide (CO$_2$) sequestration projects have been implemented all over the world. Sleipner in Norway is the first and also the hitherto longest running (20 years since 1996) CCS site in the world. Weyburn in Canada is the largest land-based CO$_2$ storage site in the world in conjunction with enhancement oil recovery (EOR) and horizontal drilling technology. It has realized injection of supercritical CO$_2$ at 5,000 tonnes (t) per day into the Mississippian reservoir under depths of around 1,450 m (Preston et al. 2005). Compared to Sleipner with the extremely favorable reservoir conditions, In Salah in Algeria is an onshore CO$_2$ storage project in low porosity/permeability settings. CO$_2$ storage at these three sites is of commercial scale or at least of demonstration scale (Michael et al. 2010). By contrast, Ketzin in Germany is the first European onshore storage site for pilot-scale CO$_2$ injection research (Martens et al. 2011). These project sites have boosted science and technology in the field of CCS remarkably.

Since mid-1980s, knowledge and experience about CCS has been accumulated from a series of EOR projects across China. However, CCS studies are still in their infancy in China. So far, no comprehensive experiences have been gained on subsurface storage of CO$_2$ due to lack of operational projects. In 2010, the China Shenhua Coal Liquefaction Co. Ltd. (CSCLC) as the field operator launched the first CCS program in the low-permeability ($<1.0 \times 10^{-14}$ m^2) formations of the Ordos Basin. Conventionally, it has been widely proposed that selection of a geological sequestration site be targeted to reservoirs with relatively high permeability and porosity, because it is more likely to ascertain success of a project by injecting CO$_2$ down into formations. For instance, Cooper (2009) suggested that reservoirs with permeability above

1.0×10^{-13} m^2 ensure CO$_2$ sufficiently accessing the pore space; however, such formations are not always available in some areas where CO$_2$ sequestration is in need. Therefore, low-permeability saline aquifers are increasingly taken into account when planning CCS projects in such areas. Eigestad et al. (2009) found that low-permeability aquifers may not be as disadvantageous as supposed in some cases. From a storage point of view, formations with high permeability are favorable due to their great injectivity. However, because the plume spreads over a larger area, there is an increased risk of CO$_2$ intersecting more permeable geologic features such as faults where leakage into shallow formations could occur (Dockrill and Shipton 2010; Jung et al. 2014; Pruess 2008).

The Ordos Basin has been identified as an inland basin in China that is a potentially favorable place for geological disposal of CO$_2$, due to its widespread deep saline aquifers under depths of 800 m; however, the formations are characteristic of low/extremely low permeability in this basin. The injectivity and injection-associated pressure buildup are therefore primary concerns at the beginning of the project. Unexpectedly, the injection operation turned out to be quite successful. The Triassic Liujiagou sandstone unit has surprisingly high injectivity when considering the overall low permeability. The wellhead injection pressure dropped from around 7 mega Pascal (MPa) at the beginning to less than 5 MPa at present and no significant pressure buildup has been observed at the site (Wu 2013; Xie et al. 2015). This phenomenon has raised increasing interest in the Chinese CCS community.

There is extensive literature reporting the numerical simulation of the aquifer-scale sequestration process for the purpose of either estimating the storage capacity (Bachu et al. 1994; Doughty and Pruess 2004; Kopp et al. 2009; Vilarrasa et al. 2010; Watson et al. 2014) or assessing the fate of CO$_2$ plumes (Jahangiri and Zhang 2011; Zhang et al. 2009; Zhao et al. 2012); however, few studies on low-permeability injection sites such as the study site here (Chenjiacun) have been reported. Previous studies analyzing this area of interest include the work of Bai et al. (2012) who applied a fast explicit finite difference method (FEFDM) to calculate the wellhead injection pressure, Chang et al. (2013) who presented results of the core-flood experiments with sandstone from the Chenjiacun site, and Li et al. (2013) who assessed the leakage risk at the same site by using the screening and ranking framework (SRF) developed by Oldenburg (2008). This has been noted in preliminary work on numerical simulation of the Chenjiacun site (Xie et al. 2015). The work is based on an early geological recognition that assumes the formation between depths of 1,690–1,615 m is extremely sealing mud (with permeability set as 1.16×10^{-18} m^2); however, the model overestimates the injection-induced pressure buildup significantly. In the present work, important field observations from the site are reported, and fundamental issues such as the plume dynamics and pressure buildup are

addressed by applying an updated numerical model to investigating the first ongoing Chinese demonstration CCS project in the Ordos Basin. More information about the site has been assimilated into the present model as further data become available and, hence, enabled further refinement. The model presented herein assumes aquitards over depths of 1,690–1,615 m, which have higher porosities and permeabilities than their previous values specified in Xie et al. (2015). Actual geological formation data obtained from the site were used in order to characterize the reservoir. This study is intended to evaluate the site performance and, hence, to provide insights into feasibility of geological sequestration of CO$_2$ in low-permeability areas.

Site characteristics

Nine inland basins in China have been identified as favorable places for geological disposal of CO$_2$, of which the Ordos Basin is of particularly interest, due to its important status as an emerging base of the coal industry of China, plus its large dimension both in terms of the distributional area and the thickness of the saline aquifers. The Ordos Basin Triassic and Permian sandstone are recognized as deep saline aquifers that have significant potential for geological CO$_2$ sequestration. Rough estimations indicate the storage capacity of the Ordos Basin for CO$_2$ would be over 10 billion t (Li et al. 2006; Ren et al. 2010). The basin, as a large-scale (250,000 km^2) inland sedimentary basin, rich in oil and gas, has been well studied geologically (He et al. 2013; Li and Li 2008; Liu et al. 2014; Qiu et al. 2014; Ran et al. 2012; Yang and Deng 2013; Yang et al. 2012, 2014); however, much work still remains in order to refine our understanding about its potential as a site for geological CO$_2$ sequestration.

Shenhua CCS project

Geological storage of CO$_2$ received large attention in China in the past decade which led to the installation of the pilot project (Shenhua CCS program) in Ordos, the Inner-Mongolia Autonomous Region of China. The Shenhua CCS project was initiated in 2007 and implemented in 2010 by CSCLC. It is the first demonstration project in China sequestrating into the deep (>1,576 m) saline aquifers massive amounts of CO$_2$ captured from coal liquefaction plants (Best and Beck 2011; Wu 2013, 2014). The injection site (110.17°E, 39.33°N, 1,330 m a.s.l.) of the Shenhua CCS project is geographically situated in the Chenjiacun village of Wulam Len town, EjinHoro county, about 40 km southeast of Ordos (Fig. 1a,b). The current site has been selected on account of various reasons including among others low population, relatively short distance to the CO$_2$ source and relatively simple and favorable tectonics. The project was designed to inject 1.0×10^5 t of CO$_2$ per year down into the saline aquifers situated between 1,576 and 2,453 m below the ground surface (bgs). The reservoir top is at a depth of
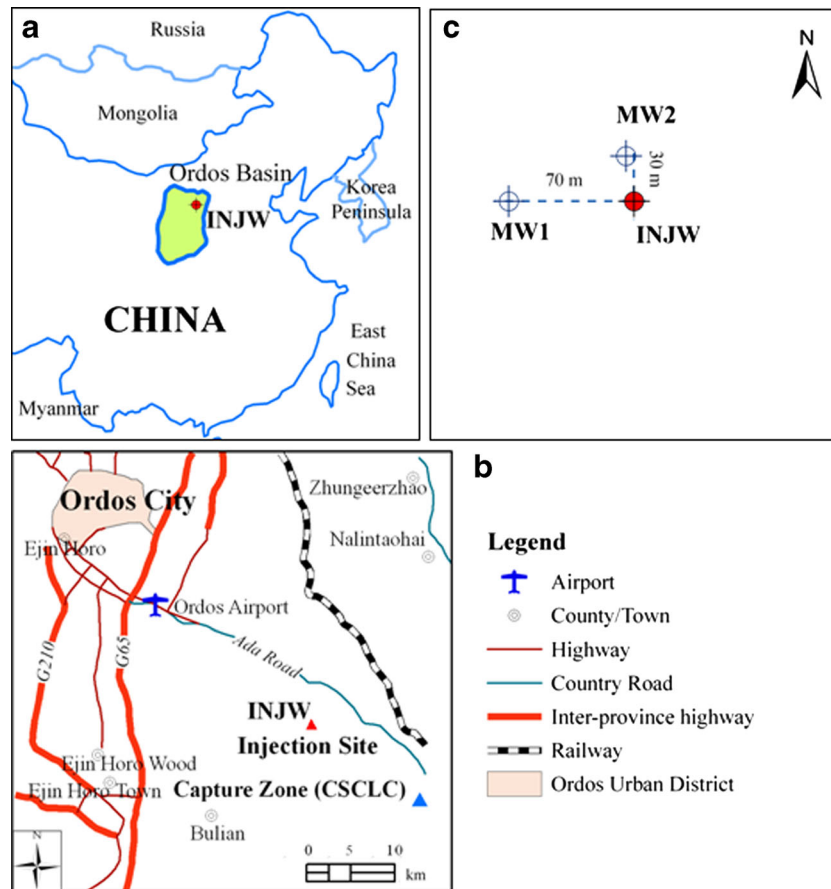
**Fig. 1** **a**–**b** Geographic location of the Chenjiacun site in the Ordos basin and **c** the relative location of the monitoring wells (*MW1* and *MW2*) to the injection well *INJW*

about 1,576 m at the current CO_2 injection well location. The injection takes place over five brine-bearing geological units that are composed of four sandstones and one carbonate and are interbedded with a sequence of mudstone caprocks (Fig. 2). As the first demonstration project in China, it was planned to run for 3 years and, hence, the goal of the project is to sequester 3.0×10^5 t of CO_2 on condition that it is stored safely. Recently, the project has been approved for a 1-year extension due to its moderate progress. The liquidated food-grade CO_2 with a purity >93.7 % is regularly transported in low temperature conditions within five tank trucks to the injection site from the capturing plant about 17 km to the southeast of the injection site (Fig. 1b). A single vertical well was drilled as the injection well (INJW) with the diameter 0.3 m and the completion depth 2,826 m. Multiple screens were perforated between the depths 1,690 and 2,453 m resulting in 88-m injecting thickness in total, to ensure success of massive injection of CO_2 at this low-permeability site (Fig. 2). To improve the injectivity and storage capacity, hydraulic fracturing was applied to two sandstone layers in the Shiqianfeng formation and two sandstone layers in the Shanxi formation, whilst acidizing was applied to four carbonate layers in the Majiagou formation; however, the observations have indicated that the effect of these stimulation measures was not as significant as expected,

particularly in the early stage due to the flowback effect of the fracturing fluid.

Furthermore, there are two monitoring wells (MW1 and MW2) nearby, with MW1 70 m to the west of the INJW responsible for pressure and temperature surveillance, and with MW2 30 m to the north for regular water sampling and vertical seismic profiling (VSP) to ascertain whether CO_2 breakthrough has occurred (Fig. 1c). The injection pressure and temperature are both monitored at the wellhead and downhole 1,631.6 m bgs in the INJW, respectively. The reservoir pressure and temperature are monitored in the MW1 at depths of 1,690.45, 1,907.45, 2,196.43, and 2,424.26 m for the Liujiagou, Shiqianfeng, Shihezi and Majiagou unit, respectively. Water samplings are conducted at various depths in the MW2. The formal injection commenced on 15 September 2011 after 49 days of trial injection to test the shut-in and restart procedures. The injection operation was characterized by varying injection rates and several shut-in phases of different durations due to maintenance of capturing equipments, contingent usage of CO_2 for conflagration or power failure. Based on Bai et al. (2012), an initial operational limit of 18 MPa was set to the wellhead pressure, to avoid fracturing, initiation of seismic events or well blow out.
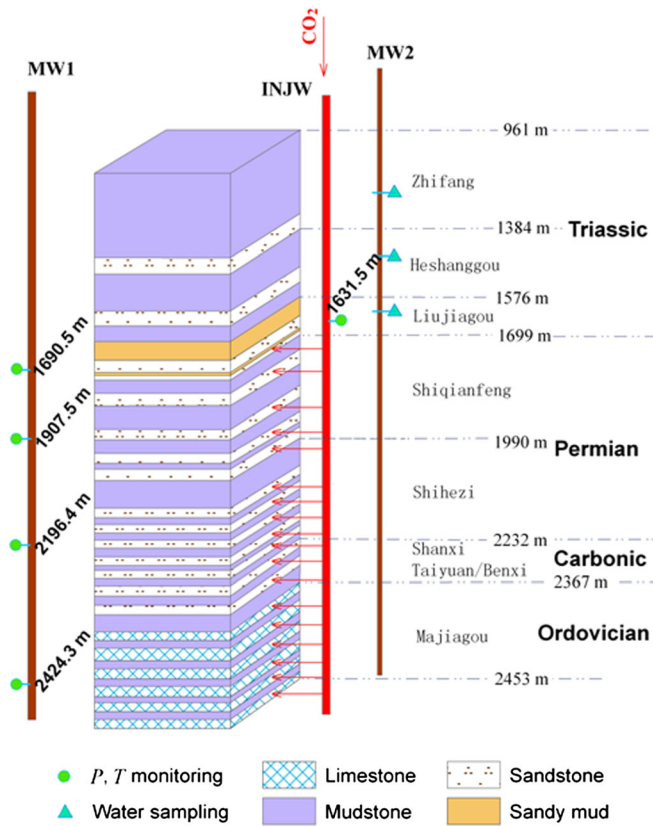
Fig. 2 Schematic diagram of the strata sequence and the wells, illustrating the location of injection layers, pressure (*P*) and temperature (*T*) monitoring and water sampling. The *dash double dot lines* suggest the formation divides and the *associated numbers* denote the depths below ground surface

Geologic setting

The injection site is situated tectonically on the Yimeng uplift of the northern part of the Ordos Basin. The strata at the site are typical of the Ordos Basin, composed of alternating mudstones and low-permeability fluvial sandstones from the Upper Carboniferous through the Lower Triassic, as well as the Ordovician limestones at the bottom. From top to bottom, the formation units are named Zhidan (C1), Anding (J2), Zhiluo (J2), Yan'an (J1), Yanchang (T3), Zhifang (T2), Heshanggou (T1), Liujiagou (T1), Shiqianfeng (P3), Shihezi (P2), Shanxi (P1), Taiyuan-Benxi (P1/C2), and Majiagou (O1). For the sake of convenience, in this report they are henceforth referred to, in sequence, as ZHD, AND, ZHL, YAN, YCH, ZHF, HSG, LJG, SQF, SHZ, SHX, TYN-BXI, and MJG. The reservoir above a depth of 2,367.4 m is dominantly fine-grained and mud-bearing fluvial sand or silt, with permeability typically ranging from 0.002 to 3.7×10^{-14} m^2 and porosity ranging from 2.5 to 12.9 %. The lower reservoir is comparatively dense carbonate (limestone), with porosity 1.7–5.6 % and permeability approximately 3.2×10^{-16} m^2. The porosity and permeability of the topmost storage reservoir (i.e., the Lower-Triassic LJG sandstone) at Chenjiacun average around 11.4 % and 1.06×10^{-14} m^2, respectively. Despite the characteristics of low permeability, the drilling operation of the INJW has encountered frequent loss of drilling mud in the Lower Triassic LJG Formation, indicating zones of

lost circulation and relatively high permeability in this aquifer. The presence of sand belts and strong heterogeneity over these depths should be responsible for this phenomenon according to the 3D-seismic interpretation. The reservoir formation slightly dips toward the northwest with a dip angle less than 2°. Geologic structures such as faults and fractures are extensively developed; however, they are mostly identified to be of minor sizes and mud-filled and, hence, are assumed to have little impact on the project. Paleochannel belts are likely developed in the Lower-Middle Permian formations (SHX and SHZ). More information about the geology of the area is found from various sources (Jiao et al. 2011; Li et al. 2013; Wu 2013).

Data and method

There are a very limited number of deep wells situated near the injection site. A 3D baseline seismic survey covering an area of 12.0 km × 8.4 km was carried out in 2010 (Xie et al. 2015). The data used in this study broadly include the borehole record, 3D seismic data, VSP interpretation, testing injection data, injection operating data, and observed pressures from the monitoring well MW1 and injection well INJW. For the reservoir configuration beyond the area with seismic measurements, data gaps were filled by extrapolating the topography such that the formation of the model top follows a weak upward

tendency from west to east, according to the geological description about the 'monocline' in this area. Hydrogeologic parameters were obtained from the analysis of the seismic and well log data. Injection has been performed for more than 3 years since May 2011, although the available operational data were only available up to January 2014 (i.e., 2.72 years) at the time of writing. The pressure observation data were available for 9 May 2011–18 December 2013. Permanent downhole monitoring system was used for INJW and MW1 to record in real time the pressure and temperature of the injection well (at 1,631.6 m) and reservoir formations (at 1,690.45 m for LJG, 1,907.45 m for SQF, 2,196.43 m for SHZ, and 2,424.26 m for MJG). The observed pressures have a nominal accuracy of ±0.02 % and a resolution of 0.05 KPa.

In this study, the observed phenomena were analyzed as the first step to figure out the reservoir behavior before/after the injection. On the second step, based on the observation analysis, numerical modeling was utilized to duplicate the injection related physics and, hence, to predict the plume behavior in the future. The subsequent observations serve as constraints to the simulation model, as described further in the following.

Field observations

The injection regime and pressure dynamics

The injection flow rates are measured with a volumetric flow meter installed at the wellhead of the injection well. The flow meter has an accuracy of ±0.35 % of the measured value. The injected mass rate of CO_2 in this study is calculated with the product of the volumetric flow rate and the corresponding density, which is estimated with the Span-Wagner correlation (Span and Wagner 1996). The cumulative mass of CO_2 injected at a certain time is then calculated by integrating the actual mass flow rates over time. Unfortunately, there are considerable data gaps in the data recorded by the flow meter. Since the total injection mass for a certain period of time is known from the loading record, the injected mass rates were gap-bridged or fine-tuned in case of inconsistency such that the cumulative injection mass for a certain period of time is equal to the mass derived from the loading record.

Figure 3a visualizes the time series of the total mass rate of the CO_2 injected during 9 May 2011–28 January 2014, along with the concurrent cumulative injection mass. The intermittent zero-value intervals indicate frequent shut-in breaks or periods during injection. The data clearly show that the injection rate overall increased with time since injection started. The maximum injection rate is 5.42 kg s^{-1}, resulting in 170,000 t/year. Up until January 2014, the cumulative mass of injected CO_2 approached 185,000 t. It is planned to increase the injection rate to accomplish the designed storage amount (300,000 t) in early 2015. Figure 3b shows the observed pressures at INJW and at MW1 for the four reservoir units. The reservoir pressure field varied, roughly between 15 and
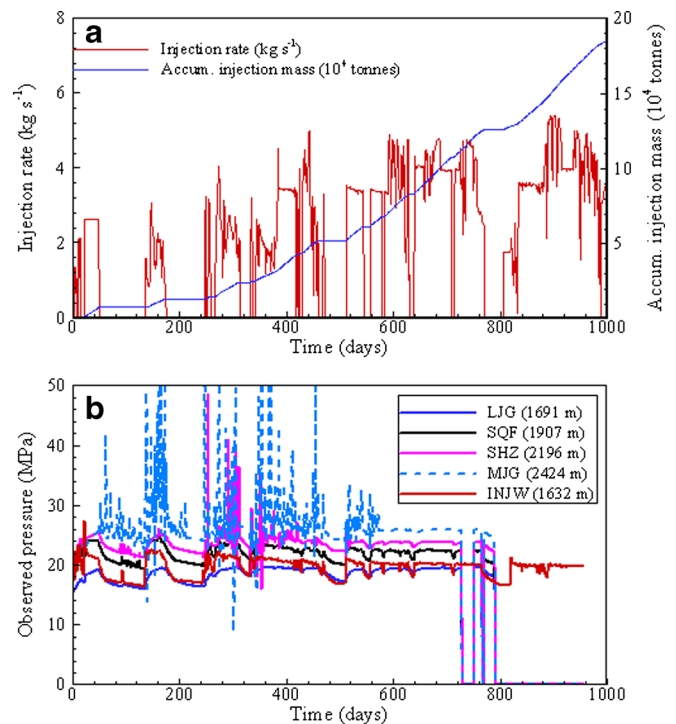
Fig. 3 The dynamics of the **a** injection mass rates and the accumulative injection mass of CO_2 and **b** the resulting observed pressures at the INJW and four reservoirs in MW1 during 9 May 2011–28 January 2014. The *values in brackets* in the legend in **b** indicate the depths where the pressures were observed

26 MPa, with zero values at 700–800 days for all the four monitored depths and extremely high values (above 50 MPa) for the MJG unit, which were interpreted as unrepresentative outliers and, thus, were not taken into account in this study. It is clear that the injection pressure stabilized around 20 MPa after around 1 year of injection and the reservoir pressures increased by 1–3 MPa due to injection. The reservoir pressures correlate with the injection rate and show almost an instantaneous response to any change in the injection operation, indicating good communication between the injection well and the monitoring well MW1.

Injectivity of the reservoirs

Reservoir injectivity characterizes the ease with which fluid can be injected into a geological formation. It is defined as the injection rate divided by the pressure difference between the injection point inside at the well base and the formation (Benson et al. 2005). The volumetric injectivity can be calculated with Eq. (1) by applying the Darcy's law:

$$J = \frac{q}{\Delta P} = \frac{2\pi kh}{\mu \ln(0.472 r_e/r_w)} \qquad (1)$$

Where q is the volumetric flow rate at the bottom of the injection well; ΔP is the pressure difference between the

injection well and the formation; k is the formation permeability; h is the formation thickness; μ is the viscosity of injected fluid (CO_2); r_e and r_w are equivalent closed formation radius and wellbore radius, respectively.

Following the definition by Eq. (1), the injectivity of a formation is mainly dependent on the permeability and thickness of the reservoir. For the reservoirs of interest (namely, the LJG downwards), the formation has four sandstone units and one limestone unit separated by mudstones. The SQF and SHZ formations have great thickness for both the storage reservoir and the caprock; however, their permeability is much lower than the overlying LJG formation. Four testing injections were performed in 2011 by injecting CO_2 at a temperature of approximately 0 °C and under pressure of around 5.16 MPa at the wellhead, down into the storage reservoirs below 1,615 m depth. Table 1 presents the percentage volumes of the CO_2 injected for each storage formation during the testing injections. It is clear that the LJG Formation is the most favorable storage reservoir for CO_2 sequestration because its injectivity contribution to the entire system averages 79.3 %. The SQF Formation would be the secondary storage reservoir for CO_2 storage, which contributes about 12.5 % of the injectivity. The contribution to injectivity in general decreases with an increasing depth (Table 1).

Pressure and temperature gradients

The atmospheric pressure and temperature at the surface of the studied area are approximately 0.854×10^5 Pa and 7 °C, respectively (Sun and Su 2012). The downhole pressure and temperature measurements before the injection reveal that the strata at the Chenjiacun site basically have the average tectonic pressure and temperature gradients. The pressure at 1,694.5 m and 2,389.3 m was observed to be 15.26 and 20.55 MPa, respectively. The resulting pressure gradient is about 0.86 MPa per 100 m from 1,076 to 2,502 m. The formation temperature follows a geothermal gradient of 26.8 °C/km, which is moderate when compared to the southern and northern part of the Western Canada Sedimentary Basin as reported in Bachu (2003). The temperature at 1,712.6 and 2,389.3 m was 53.0 and 72.5 °C, respectively (Fig. 4). For temperatures greater than 31.1 °C and pressures greater than 7.38 MPa, CO_2 behaves like a gas but has a "liquid" density and is named supercritical fluid (Bachu 2003; Pruess 2005). The minimum depth for

Table 1 Percentage volumes of the injected CO_2 for the five storage formations (Fm.) during the testing injections. *Ave* average

| Fm. unit	Test 1	Test 2	Test 3	Test 4	Ave.
LJG	79.4	81.8	77.3	78.6	79.3
SQF	12.3	10.8	13.8	12.9	12.5
SHZ	5.0	4.0	5.8	3.6	4.6
SHX	0.00	3.4	0.0	0.1	0.9
MJG	3.3	0.0	3.1	4.8	2.7
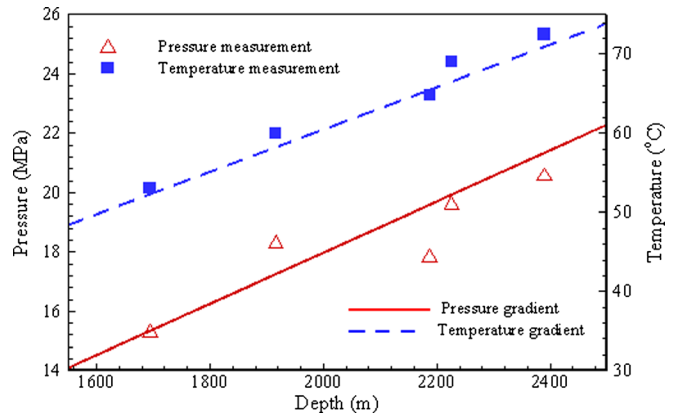
**Fig. 4** Variation of pressure and temperature with depth below the surface

CO_2 to be in a supercritical state is estimated to be 903 m for this site, based on the afore-mentioned pressure and temperature data, which indicates a supercritical reservoir environment at the Chenjiacun site for CO_2 sequestration or storage.

Distribution of porosity and permeability

Geological complexity leads to heterogeneity of rock properties. From a carbon sequestration standpoint, both porosity and permeability influence the migration of the CO_2 saturation plume in the storage formation. The porosity and permeability fields illustrated in Figs. 5 and 6 are based on correlation relationships between the logging data in the INJW and the 3D seismic data. For more details the readers are referred to Wu (2013) and Xie et al. (2015). From Figs. 5 and 6, the reservoir is identified as a highly heterogeneous medium with low permeability and porosity. The porosity and permeability vary from 0.01 to 20 % and 1.0×10^{-21} to 7.3×10^{-14} m^2, respectively. As indicated in Fig. 5, both the porosity and permeability have a tendency to decrease downwards with the depth, which is thought to be due to the effect of compaction. Figure 6 illustrates the planar distribution of the porosity and permeability in the LJG injection layer, with the layer-averaged value
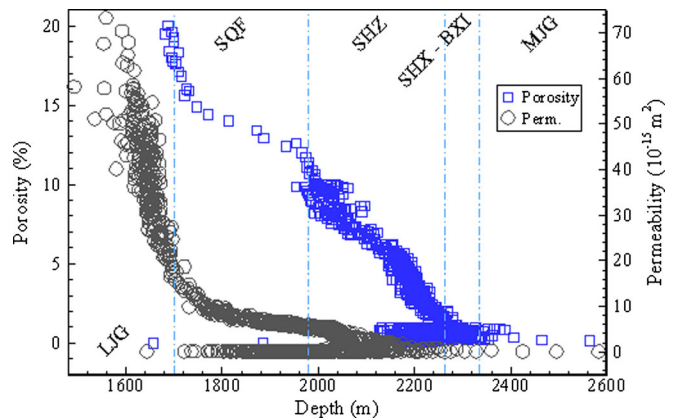
Fig. 5 Variation of porosity and permeability against the depth determined by logging in the INJW and 3D-seismic interpretation
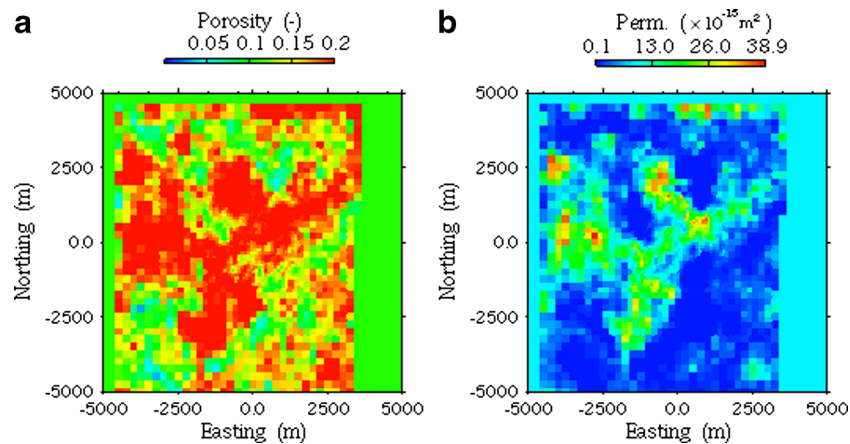
Fig. 6 Patterns of **a** porosity and **b** horizontal permeability in the LJG injection layer. The injection well (INJW) is centered in the simulated area shown

assigned for the area beyond the measurement. It can be seen that there is a considerable proportion of the area that is characterized by relatively high porosity and permeability. This highly permeable area stretches somewhat in the NE–SW direction (Fig. 6). Such distributional characteristics of the porosity and permeability may play an important role in the interpretation of saturation plume migration.

Spreading of the CO_2 plume

Vertical seismic profiling (VSP) surveys have been conducted three times for the purpose of CO_2 monitoring at MW2 since May of 2011. Processing of the time-lapse VSP data found that the growth of the injected CO_2 plume is roughly circular in the horizontal plane (Wu 2013). The effect of heterogeneity on the plume distribution is not as prominent as expected, probably because of generally slow and, hence, even spreading due to low permeability and gentle reservoir topography. The lateral extent of the CO_2 plume in the injected interval is some 350 m away from the injection point at approximately 2 years after the commencement of the injection (Chen et al. 2014). However, since the downhole geophones were emplaced 500+ m above the injected interval to avoid corrosion due to potential CO_2 leak, the interpretation presented by Chen et al. (2014) could not distinguish the plume sizes between the injected layers.

Numerical simulation

Geological model

The geological model is based on information from borehole measurements and seismic data at the site. The upper part of the reservoir is composed of a sequence of permeable sandstone/siltstone strata with alternating low-permeability mudstones/coal beds. In contrast, the lower part of the reservoir consists of fractured carbonate strata

interbedded with mudstones. An early model developed in the work of Xie et al. (2015) characterizes the formation between 1,690 and 1,699 m as the primary storage reservoir for the Chenjiacun site; however, CO_2 was detected in well MW2 at depths between 1,539 and 1,544 m. Following the relevant experts' suggestion, in the present work, the depth interval 1,615–1,699 m was set as the storage reservoir in the LJG Formation unit. The depth interval 1,547.8–1,615 m was set as the overlying caprock because a set of sandy mudstones were identified there (Fig. 2). The structural model for this study has a lateral extent of 12 km × 12 km and an average vertical thickness of 800 m. The bottom of HSG (1,547.8–1,576 m) was chosen as the model top because there is a mud layer immediately above the LJG Formation (Fig. 2). The accumulative thickness of the storage reservoirs is 218.6 m between depths 1,547.8 and 2,453.0 m, separated by 686.6 m of mudstones at various depths. The reservoir is sandstone/siltstone for the upper 187.4 m of thickness. The lower 31.2 m-thickness of the reservoir is comparatively dense carbonate (limestone). The interbedded mudstones act as barriers for vertical flow. Semi-permeable formations are assumed at depths 1,680–1,690 m and 1,576–1,615 m because alternating thin layers and patches of sandstones and mudstones exist over these depths and, hence, hydraulic communication is possible across these layers. The formations are heterogeneous in porosity and permeability.

Model gridding

The model grid configuration is exactly the same as that used in Xie et al. (2015), except for its larger extent of the present model domain. Radial grids were adopted for discretizing the near-well field within distance of 1,500 m, whilst square grids were used in the far field. Fine grid spacings with the smallest size to be 0.30 m were used for the vicinity of the injection well to obtain more accurate results. Vertically, 22 geological properties were assigned to 50 grid layers, which include 19 sandstones, 1 sandy mud, and 1 carbonate aquifer interbedded with mudstone

confining layers. The model established herein ends up with 175,600 grid cells.

Model assignments

ECO2N (Pruess 2005), a TOUGH2 fluid property module for mixtures of water, salt and CO_2 is used to simulate the injection-associated physical processes. The simulator describes the fluid flow with Darcy's Law for multiphase flow extension. The target reservoir formations occur extensively in the basin and are therefore represented as laterally infinite acting reservoirs in this study. Fixed pressure boundaries are specified in the lateral domain, whilst the entire system is impermeable above and below according to the geologic model. The formation properties such as permeability and porosity are assigned based on the 3D seismic interpretation and logging data. The ratio of horizontal to vertical permeability is assumed to be 10 for all the formation rocks. All the interbedded caprocks are assumed to be lithologically identical to the top seal.

The initial pore pressure was applied using a pore pressure gradient which was consequently adjusted to the adopted initial pore pressure being about 15.26 MPa at 1,694.5 m depth, based on the measured value. The initial temperature varies linearly with a geothermal gradient of 26.8 °C/km from 37.3 °C at the model top layer to 72.6 °C at the bottom layer. Diffusion in aqueous and gaseous phases is neglected because it is negligible over the simulated time frame of 103 years. It is assumed that the formations are initially water-saturated. The reservoir brine has a salinity of 3 % (i.e., 30 g salt per kg water) based on the measured value. The formations are assumed to be free of gas phase initially. Relative permeabilities and capillary pressures are calculated using van Genuchtan-Mualem functions (Mualem 1976; Van Genuchten 1980) and van Genuchten functions (Van Genuchten 1980), respectively (Fig. 7). The residual water
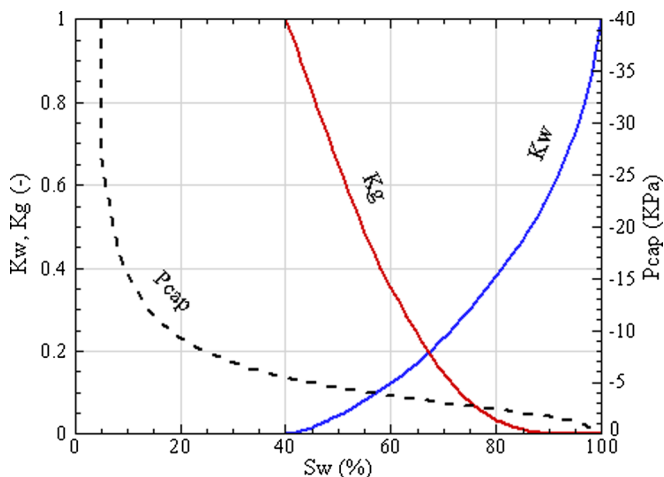
saturation and residual gas saturation are estimated to be 35–50 and 5 % respectively, according to the consensus of the project team. The pore compressibility was derived from the formation tests in INJW, while the entry capillary pressure was determined by literature survey (Chang et al. 2013; Pruess 2005). Both the maximum water and CO_2 saturation are assumed to be 1.0. The parameter 'm' in van Genuchten's notation is set to 0.45 by convention. Table 2 summarizes the main inputs of the model for the simulation modeling.

Simulations were run under isothermal conditions for 3.65 years of injection and followed by 100 years of post-injection simulation, because understanding CO_2 plume evolution during the post-injection period is of importance for a sequestration project. The injection rates shown in Fig. 3 were adopted in the model for the first 2.73 years (or 995 days). However, the injection rates were simply specified as 3.97 kg s^{-1} for the following injection period such that the total cumulative mass of CO_2 injected is 300,000 t by 3.65 years. Mineral trapping of CO_2, which may occur due to the dissolved phase CO_2 contacting the rock mineral surfaces, is not considered in the present study. The model was calibrated by adjusting the parameters such as absolute permeability and relative permeability and capillary associated coefficients to match (1) the monitored pressure dynamics as shown in Fig. 3, (2) the injectivity contribution for each storage reservoir manifested by the testing injection (Table 1) and (3) the areal distribution for the injected CO_2 derived from the VSP imaging, which concludes that the migration radius of the CO_2 is around 350 m laterally after the 2-year injection (Chen et al. 2014). It should be noted that up to 8 reference times (i.e., 1.00, 2.73, 3.65, 13.65, 33.65, 53.65, 73.65 and 103.65 years) were chosen for model output visualization on account of the fact that 1.00 and 3.65 years provide information in the middle and at the end of injection respectively, whereas 2.73 years represents the end of duration where the operational data are available; for the remaining times, just a normal practice was followed.

Dynamics of the CO$_2$ plume

The migration of the CO_2 plume is one aspect of the displacement process in the subsurface that is relevant for assessing the safety aspects of geological sequestration (Berg et al. 2013; Esposito and Benson 2010). In this report, the plume front is defined with the CO_2 saturation cutoff being 0.05. The plume is roughly circular in the planar direction for the early part of the injection period. As time proceeds, the plume tends to develop a more irregular (oval) shape due to the effect of heterogeneity. As with the permeability and porosity fields, the plume within the LJG reservoir has a geometry oriented somewhat in the NE–SW direction (Figs. 6 and 8). From Fig. 8, it can be seen that the distribution of CO_2 saturation is different in the late part of the post-injection period. This is primarily due to the saturation perturbation

Fig. 7 Relative permeability and capillary pressure curves plotted against brine saturation for the model simulation. *Kw* and *Kg* denote relative permeability of brine and CO_2, respectively. *Pcap* represents capillary pressure. *Sw* indicates effective brine saturation

Table 2 Hydrogeologic parameters for the different formation units in the model

| Fm. units	ρ (kg m^{-3})	Ø (%)	k (10^{-15} m^2)	C (10^{-10} Pa^{-1})	P_0 (KPa)	S_{wr} (−)
SEALS	2,600	0.01	1.16E-05	0.95	383.14	0.55
HSG	2,500	2.5	0.01	1.10	11.22	0.55
LJG1-LJG4	2,400–2,500	2.5–11.4	0.01–10.60	1.10–6.80	3.27–11.22	0.40–0.50
SQF1-SQF7	2,400–2,500	6.1–12.9	0.11–2.96	3.70–6.70	5.08–10.85	0.45–0.50
SHZ1-SHZ5	2,400–2,600	8.0–12.6	0.36–2.70	6.38	5.46–10.08	0.45–0.50
SHX1-SHX3	2,500–2,600	3.6–11.3	0.01–2.02	1.00–6.53	6.62–11.99	0.50
MJG	2,700	3.5	0.32	9.28	10.46	0.50
INJW	2,600	99.9	200.00	9.50	2.78	0.30

ρ rock density, Ø porosity, k absolute permeabilities in X and Y directions, C pore compressibility, P_0 capillary entry pressure, S_{wr} residual water saturation

raised by the reservoir topography especially when CO_2 distribution is dominated by buoyant forces after the injection ceased. Dissolution of CO_2 would be another important reason for these changes after the end of injection. As will be discussed in section 'Storage safety', the dissolution effect becomes more significant during the post-injection period. Figure 9 illustrates the $Y=0$ vertical profiles of the CO_2 plume at various times since injection. The dominating feature in Fig. 9 is that the injected CO_2 is substantially maintained within a 19-m interval (about 1,680–1,699 m) in the lower LJG unit, due to the presence of mudstone above it. The remainder of the injected CO_2 is sequestered in the SQF unit at depths of around 1,754, 1,920, 1,944 and 1,986 m, and in the SHZ unit at depths of around 2,107 and 2,171 m. The CO_2 saturation attenuates outward with increasing distance from the injection well. Statistics from the simulation results reveal that the average CO_2 saturation within 500 m of the injection well was approximately 0.23 at 1 year and approached its highest value of 0.39 when the injection terminated. Figure 10 plots the development of the plume size (which herein is defined as the maximum lateral extent of the plume) in the LJG unit with the time lapse since the onset of injection. The lateral extent of the CO_2 plume in the LJG unit is some 233 m at 1 year after the commencement of injection. The CO_2 plume expands to 658, 913, and 1,013 m at 3.65, 53.65, and 103.65 years after the commencement of injection, respectively. It follows that the injected CO_2 resides within approximately 1,000 m of the INJW during the simulation period due to the characteristics of low-permeability and flat formations at the Chenjiacun field; therefore, the migration of the
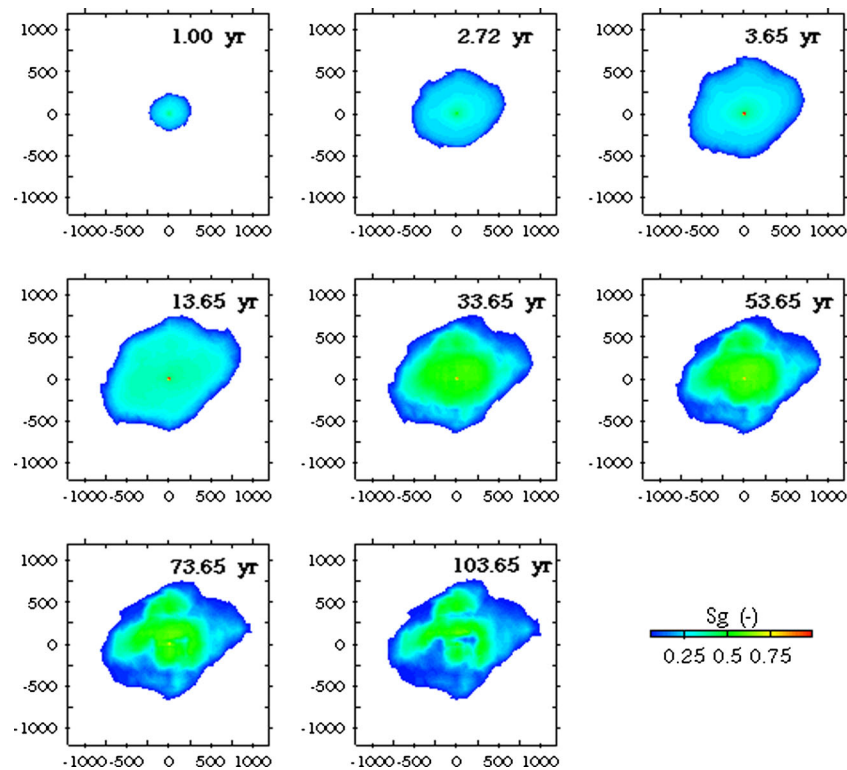
Fig. 8 Top view of the simulated CO_2 saturation (Sg) plume (with saturation cutoff 0.05) in the LJG unit at various times. The units for the plot axes are meters (m)
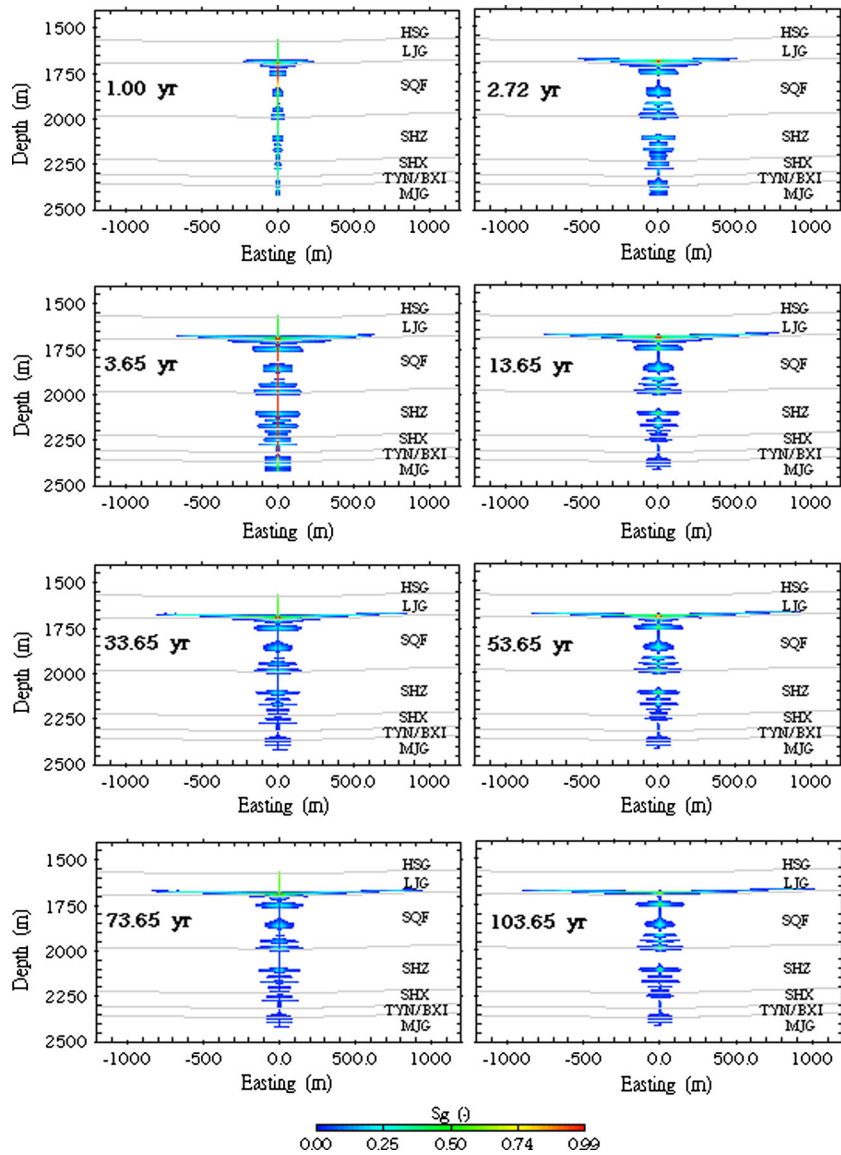
Fig. 9 Vertical profiles of the simulated CO_2 saturation (Sg) plume at various times. The *grey lines* indicate the divide of formation units. The units for the plot axes are meters (m)

injected CO_2 in the reservoirs is expected to be quite limited.

Pressure dynamics

The pressure response to injection of CO_2 is the most important concern, since a high injection pressure and large-scale pressure buildup can reduce the injectable amount of CO_2 in the long term (Zhou et al. 2008). Figure 11 illustrates the simulated pressure dynamics at the monitored depths within the injection well and reservoirs from 9 May 2011 to 28 Oct. 2016. For the first 2.72 years (995 days), both the injection and reservoir pressures fluctuate due to alternation of open-up and shut-in. The almost simultaneous response of the reservoir pressures to the injection operation suggests a good hydraulic connection between the injection well and monitoring well. After that, the pressures in the injection

well and the LJG unit stabilize due to the constant injection assumed throughout that period. After 3.65 years (i.e., 1,332 days), the injection stopped, which was accompanied by quick pressure drops due to compressibility effects and dissolution of CO_2. During the entire simulation period, there is only a very small pressure signal observed in the top seal, indicating that the thick low-permeability caprock acts as an effective barrier with the current injection plan over the simulated 103.65 years.

The pressures calculated by the model show relatively good agreement with the observed data (Fig. 12). While the model underestimates the pressures for the lower reservoirs, the overall performance of the model developed is justified since the pressure match for the injection well (INJW) and the LJG unit is basically good. Bear in mind that the LJG unit acts as the overwhelmingly primary storage reservoir for the CO_2 injected at Chenjiacun. Higher observed pressures, especially in the
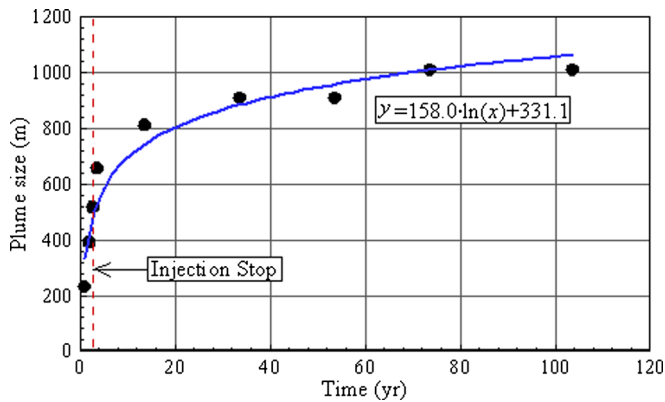
Fig. 10 Evolution of the simulated CO_2 plume size in the *LJG* reservoir plotted against the time after the onset of injection. The *vertical red dash line* indicates the location of the time point when the injection ceased

SQF and SHZ formations (Fig. 12b,c), could be related to the simulations not accounting for packers used to isolate the measurements in the field. Interestingly, the top packers mounted in the monitoring well, MW1, are quite close to the measurement point for the SQF and SHZ, while in the LJG the monitoring point is relatively far from the packers. The presence of the packers could make the monitoring position further overpressurized. Still, one cannot rule out other reasons that are possibly important but still not clear at this stage. An in-depth analysis of this issue is needed through a follow-up study. Furthermore, possible errors in monitoring data as shown in Fig. 12c,d should always be taken into account.

Pressure buildup

An important consideration in operation of CCS projects is the pressure buildup during injection. Knowledge of the scale and magnitude of the pressure buildup is essential for an accurate assessment of the sequestration safety and sustainable injectivity. Figure 13 presents the vertical profiles of pressure buildup at various times after the commencement of injection. Compared to the saturation
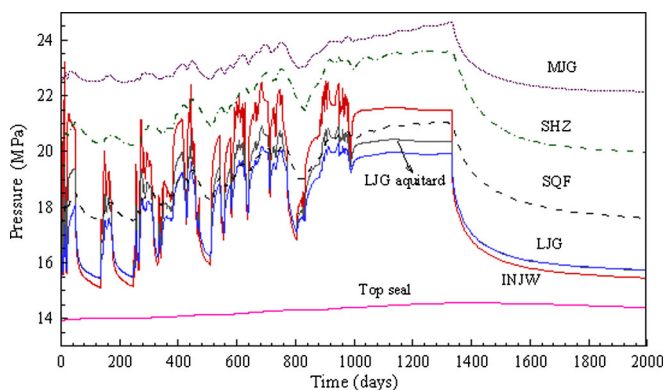

Fig. 11 Simulated pressure dynamics from 9 May 2011 to 28 October 2016

plume size as demonstrated in Fig. 9, the scale of the pressure buildup is much larger. With increasing injection time, the elevated pressure propagates further out into the formation and extends to about 3,000 m (Fig. 13c). During the 3.65-year injection, the simulated pressure reaches its highest value of 21 MPa, causing about 7 MPa of pressure buildup in the injection center and approximately 5 MPa of pressure buildup in the near field of the primary reservoir (i.e., the LJG unit). Similar but relatively lower pressure buildup is observed for the remaining three reservoirs. The elevated pressure dissipates quickly after the injection ceases. The pressure buildup caused by injection is hardly noticeable after 10 years into the post-injection period (Fig. 13d). As will be discussed further in the following, the current magnitude of the pressure buildup would not give rise to the formation of highly permeable fractures within or near the injected formation.

Reservoir injectivity

In many cases, permeability is seen as a measure of injectivity because the permeability of the storage formation determines the feasible rate of injection into it. As such, for a given identical period of time, reservoir injectivity can be assessed by investigating the cumulative mass of CO_2 injected. Figure 14 presents the simulated evolution of cumulative CO_2 mass injected into each formation unit over the simulation period. During the 3.65-year injection, CO_2 mass increases at a different rate for each formation unit due to their differing injectivity. With increasing injection time, the cumulative CO_2 mass injected into the LJG reservoir increases markedly and approaches approximately 210,000 t at the end of the injection, accounting for 70 % of the total injection amount. By contrast, CO_2 accumulation in the lower reservoirs proceeds much more slowly, indicating comparatively lower injectivity. During the post-injection period, the total CO_2 mass in the subsurface is unchanged. Interestingly, however, the CO_2 mass increases considerably in the LJG unit, accompanied by CO_2 loss in the lower reservoirs (Fig. 14). This is because the permeability of the LJG reservoir is significantly greater than the remaining reservoirs. Once the injection stopped, the pressure in the LJG reservoir dissipates more quickly (Fig. 11). Therefore, the injected CO_2 in the lower reservoirs migrated upward driven by buoyancy to the upper locations via the wellbore.

As described in the previous, the collected testing injection data (Table 1) suggest that the LJG reservoir has approximately 79 % of the injectivity of the entire reservoir system, followed by the SQF unit, which accounts for some 12 %. Figure 15 presents the evolution of simulated CO_2 mass percentages injected into each formation unit, indicating the contribution of each reservoir to the entire injectivity of the Chenjiacun site. By comparing with the testing injection data shown in Table 1, it can be seen that the model-estimated percentages are basically close to the testing injection results. The LJG unit acts as the primary storage reservoir of the
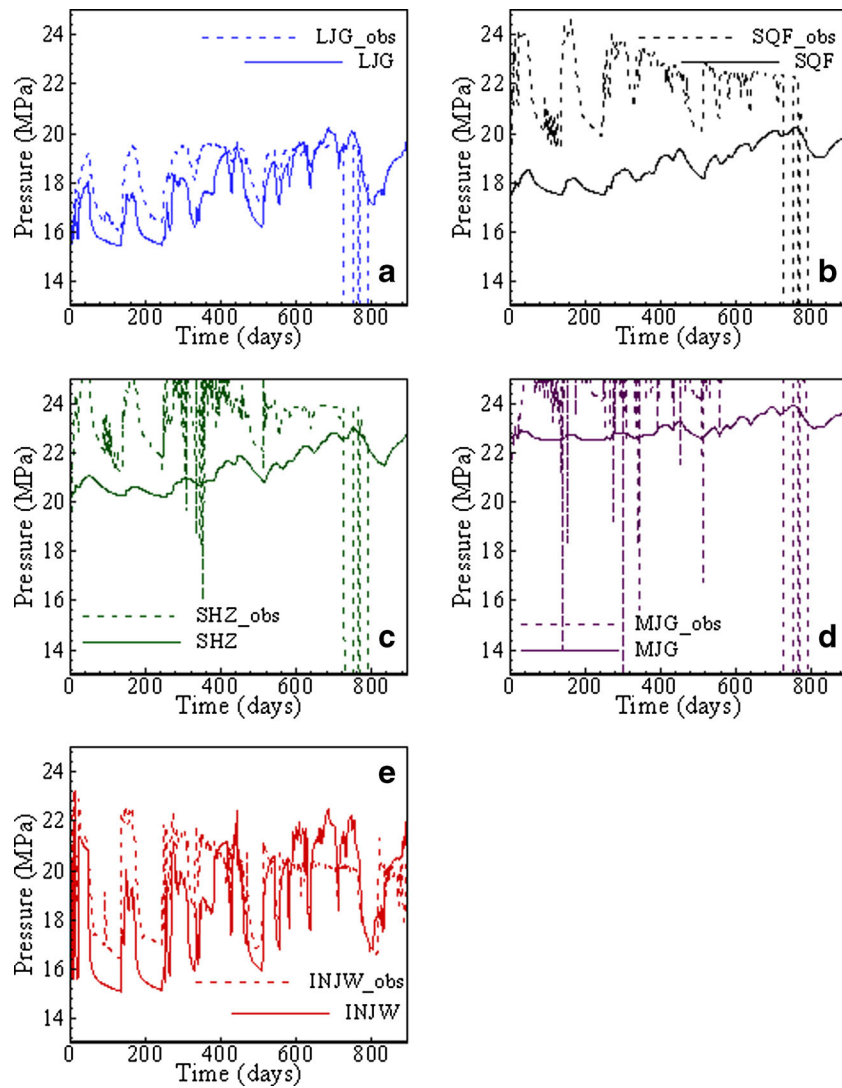
Fig. 12 Comparison between the simulated and observed pressures from 9 May 2011 to 28 January 2014 for units **a** LJG, **b** SQF, **c** SHZ and **d** MJG, and **e** injection well INJW

Chenjiacun site since around 80 % of the injected CO_2 will eventually enter this formation.

Discussion

Storage safety

As the first demonstration project in China, storage safety is of particular concern because it directly determines if this program is eventually successful. Firstly, the caprock integrity under the injection condition is crucial for the storage safety of a site. Geomechanical experiments on core samples are supposed to be performed to support an accurate safety assessment; however, these experimental results were not available for this study. Since the study uses formation fracture coefficients suggested by the project team based on an integrated analysis of the well log and stimulation operation, the first step was to estimate the fracture pressure by the product of the hydrostatic pressure and the formation fracture coefficient. After that,

the safety of the sealing cap was examined by comparing the simulated reservoir pressures with the corresponding fracture pressures under injection conditions. Figure 16 presents the distribution of reservoir pressures at the end of the injection (denoted by grey dots) and estimated fracture pressures based on the formation fracture coefficients (denoted by red squares). It can be seen that the fracture pressure for the upper part of the formation follows a fracture gradient of 20 MPa/km, which is the upper limit of the range from 12 to 20 MPa/km suggested by Crain (2000). The fracture pressure at the depth of the top seal surface was extrapolated to be approximately 33 MPa. As illustrated in Fig. 16, despite the reservoir pressure becoming higher than the hydrostatic pressure due to the injection, it remains far lower than the fracture pressure; therefore, the proposed injection scheme (with the maximum injection rate approximately 5.4 kg/s) would not threaten the integrity of the sealing formation at the Chenjiacun site.
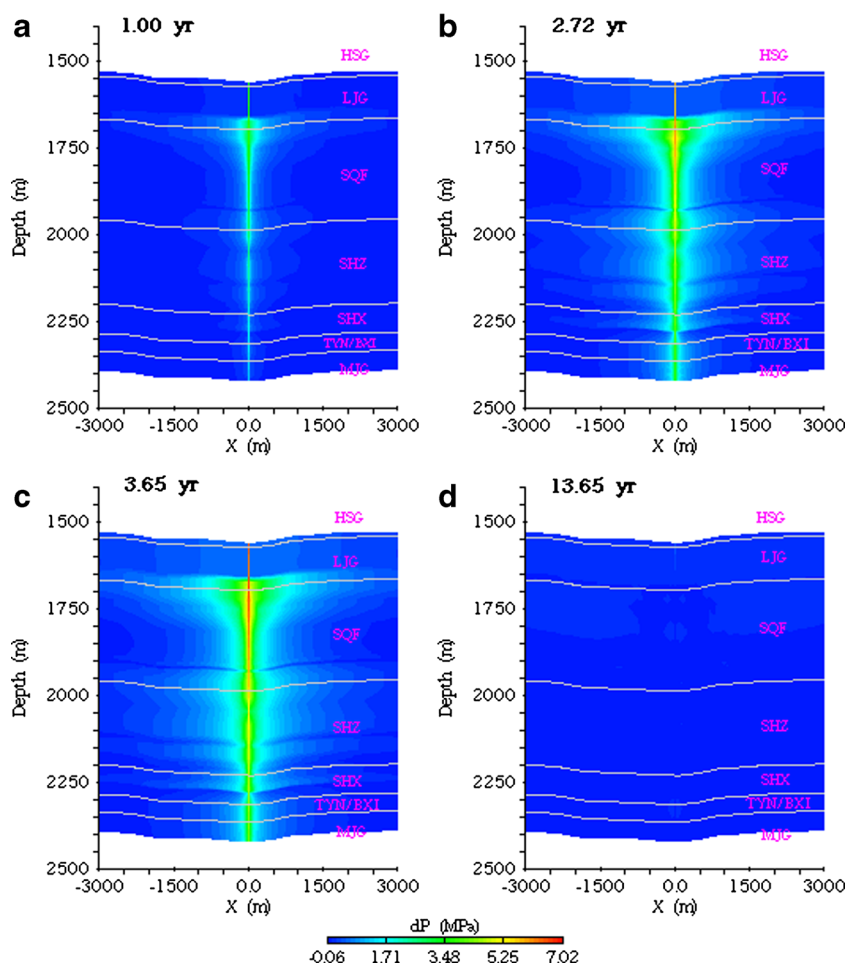
Fig. 13 **a–d** Pressure buildup (d*P*) at various times after the commencement of injection (with 7× exaggeration for the vertical axis)

Secondly, trapping forms of the injected CO_2 in the storage formation is another important concern, particularly for permanent sequestration. From a storage safety perspective, both trapped and dissolved forms of CO_2 are

the most desirable forms of storing CO_2 for long-term periods. By contrast, CO_2 as a free mobile gas will be the least desirable form, because it can potentially escape from the reservoir and ultimately return to the atmosphere. Gaseous CO_2 has strong buoyancy and this characteristic
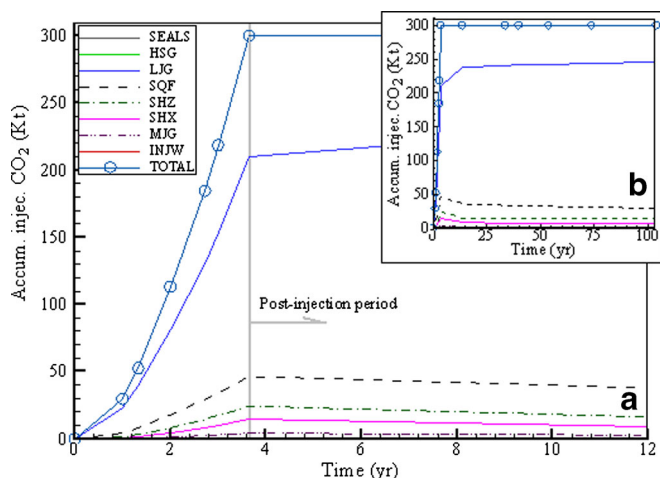
Fig. 14 **a** Accumulative mass of CO_2 injected for each formation unit evolving against the time after the onset of injection. **b** Shows the overview of the graph over the entire 103.65 years of simulation period. The values for the *SEALS*, *HSG* and *INJW* are too low to be visible on the plot
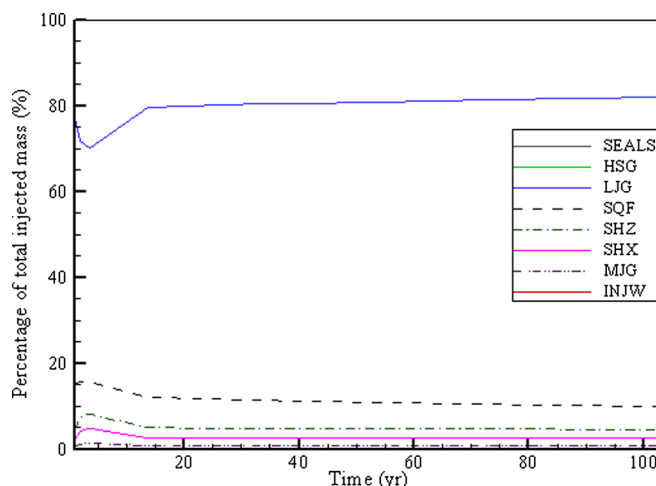

Fig. 15 Percentages of the total injected CO_2 mass for each formation unit during the simulation period. The values for the *SEALS*, *HSG* and *INJW* are too low to be visible on the plot
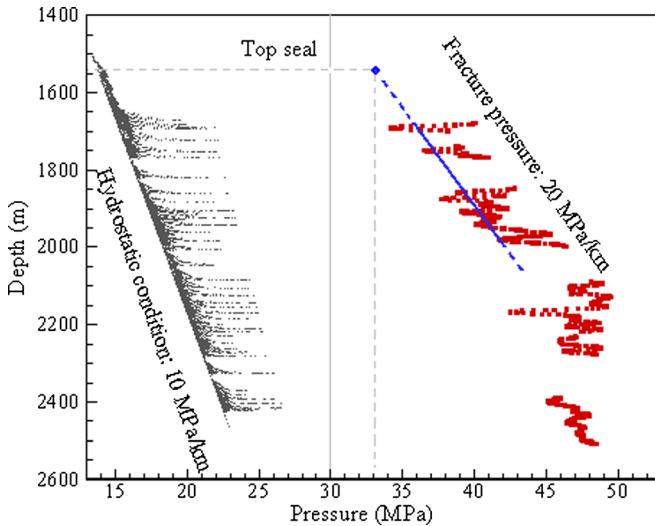
Fig. 16 Reservoir pressures (*grey dots*) and fracture pressures (*red squares*) with the extrapolated fracture pressure at the top seal formation (*blue dots*). The *horizontal and vertical broken grey lines* indicate the location of the top seal and the corresponding extrapolated fracture pressure, respectively

raises the most concern about CO_2 leakage. Ideally, the most desirable situation would be that all the injected CO_2 is dissolved into the formation water. Figure 17 plots the percentages of dissolved CO_2 injected into each formation unit over the simulation period. When supercritical CO_2 is injected down into the formation, only 20–30 % of the injected mass is dissolved in the resident formation brine. After the injection ceases, however, the percentage of dissolved CO_2 becomes much higher as more CO_2 dissolution occurs when more gaseous CO_2 contacts the formation brine during its ascent due to pressure drop. The simulation results show that 27.4 and 52.9 % of the injected CO_2 will be dissolved into the aquifer brine at 3.65 and 103.65 years respectively (Fig. 17). This means that the total dissolved CO_2 mass is expected to be approximately 82,202 t at the end of the injection, and would be increased to 158,741 t after 100 years post-
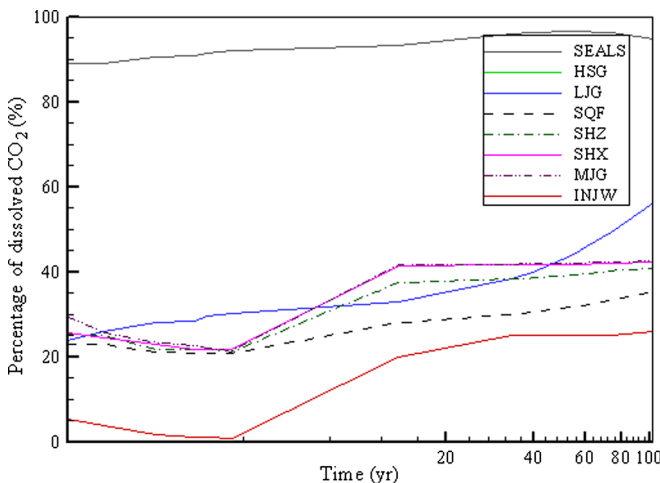
Fig. 17 Percentages of dissolved CO_2 in the injected mass for each formation unit. The values for the *HSG* are too low to be visible on the plot

injection. It should be noted that complete CO_2 dissolution in formation water potentially needs hundreds of years (Ennis-King et al. 2005; McPherson and Cole 2000). In the long run, a part of this dissolved carbon may be permanently sequestered as a mineral phase, the remaining mass being redistributed within the formation brine via advection and diffusion (Law and Bachu 1996; Saripalli and McGrail 2002).

While there is still a considerable amount of free phase CO_2 remaining within the reservoirs, the possibility of CO_2 escaping to the atmosphere through the mudstone caprocks should be very low because there is a sequence of caprock layers interbedded into the aquifers, and more importantly, the thickness of the top seal is 349 m. Van der Zwaan and Gerlagh (2009) proposed that a CCS operation is valuable when CO_2 leakage is lower than 2 % of the injected volume. The modeling results of this study reveal that only 0.02 % of the injected CO_2 enters into the caprock layers (Fig. 15, 0.02 % is too low to be visible on the plot).

Model uncertainties and limitations

Modeling underground CO_2 storage involves many conceptual and quantitative uncertainties (Oladyshkin et al. 2011). In this study, there are three major sources of uncertainty and limitations. Firstly, while the vertical reservoir geometry was derived from the core and well log data, it is somewhat uncertain, particularly in terms of defining sealing formations. In the early stage of the project, the formation between 1,690 and 1,615 m depth was interpreted as sealing caprock. However, leakage of CO_2 has been detected from the perforated casing above 1,615-m depth in monitoring well MW2, indicating the original interpretation was incorrect. The geologic model presented here is based on the current consensus within the project team, where it is proposed that the formation between 1,690 and 1,615 m depth is more likely to be permeable sands/silts. The geometry related uncertainties are also due to extrapolation of the formation topography, as the seismically investigated area did not cover the entire model domain.

Secondly, the transient injection rates specified in the model are an approximation of the observed flow rates. The mass rates of CO_2 injected for a certain time specified in the model are actually a result of gap-bridging based on the loading records of the trucks for CO_2 transportation. This implies that the injected mass rate could be considerably different with the actual value for a specific time. This could be a major reason for the relatively poor match of the pressure dynamics.

Thirdly, the present model was loosely calibrated with the VSP interpretation on the plume dynamics. It should be noted that, while time-lapse VSP monitoring of CO_2 has been applied for most of the CCS fields (e.g., Sleipner and Weyburn), quantitative estimates based on this technology, as Lumley (2010) suggested, are still challenging.

Conclusions

Updated observations from the first Chinese CCS demonstration site at Chenjiacun are analyzed for better understanding of the injection regime and reservoir behavior. The field observations over the past 2.72 years are characterized by low-pressure buildup and stabilizing tendency of the injection pressure. A simulation run of the model for the past 3 years of injection showed that the Triassic LJG sandstone in the upper part is the primary reservoir for CO_2 storage, which provides approximately 80 % of the injectivity of the site. By contrast, the injectivity in the deeper limestone reservoir (Ordovician MJG unit) is very small. The Triassic HSG mudstone formation above 1,576-m depth serves as the regional confining formation, which provides an effective permeability and capillary barrier to prevent CO_2 upward migration. The saturation plume of the injected CO_2 is observed to be laterally irregular or roughly ellipse shaped, oriented somewhat in the NE–SW direction. The lateral plume size in the LJG reservoir is expected to be 658 m by the end of injection when the designed storage amount of 300,000 t CO_2 is accomplished. The plume would expand to approximately 1,000 m after 100 years of storage. The injection caused pressure buildup within a radial area of about 3,000 m from the injection well. The reservoir pressure buildup could be mostly lower than 5 MPa for the suggested injection plan, which is slightly overestimated but still far below the fracturing pressure of the formation.

Despite the preliminary findings presented herein, this study helps to identify the most favorable formation for large-scale geologic CO_2 sequestration in this area. Operation of this project and its associated recognitions and experiences serve as an essential part of planning for the implementation of CO_2 sequestration projects in similar settings across China.

References

Bachu S (2002) Sequestration of CO_2 in geological media in response to climate change: road map for site selection using the transform of the geological space into the CO_2 phase space. Energy Convers Manag 43:87–102

Bachu S (2003) Screening and ranking of sedimentary basins for sequestration of CO_2 in geological media in response to climate change. Environ Geol 44:277–289

Bachu S, Gunter WD, Perkins EH (1994) Aquifer disposal of CO_2: hydrodynamic and mineral trapping. Energy Convers Manag 35:269–279

Bai B, Li X, Liu M, Shi L, Li Q (2012) A fast explicit finite difference method for determination of wellhead injection pressure. J Cent South Univ 19:3266–3272

Benson SMP, Cook P, Anderson J, Bachu S, Nimir HB (coordinating lead authors) et al (2005) Underground geological storage. In: IPCC special report on carbon dioxide capture and storage, chapter 5. Intergovernmental Panel on Climate Change, Vienna

Berg S, Oedai S, Ott H (2013) Displacement and mass transfer between saturated and unsaturated CO_2-brine systems in sandstone. Int J Greenhouse Gas Control 12:478–492

Best D, Beck B (2011) Status of CCS development in China. Energy Procedia 4:6141–6147

Chang C, Zhou Q, Xia L, Li X, Yu Q (2013) Dynamic displacement and non-equilibrium dissolution of supercritical CO_2 in low-permeability sandstone: an experimental study. Int J Greenhouse Gas Control 14:1–14

Chen Y, Li YL, Wu JJ, Du J, Li XF, Wang Y (2014) CO_2 monitoring with time-lapse VSP in China Northwest. Paper presented at the Fourth EAGE CO_2 Geological Storage Workshop: Demonstrating Storage Integrity and Building Confidence in CCS, Stavanger, Norway, 22–24 April 2014

Cooper C (2009) A technical basis for carbon dioxide storage. Energy Procedia 1:1727–1733

Crain ER (2000) Crain's petrophysical handbook, Spectrum. https://www.spec2000.net. Accessed May 2015

Dockrill B, Shipton ZK (2010) Structural controls on leakage from a natural CO_2 geologic storage site: central Utah, U.S.A. J Struct Geol 32:1768–1782

Doughty C, Pruess K (2004) Modeling supercritical carbon dioxide injection in heterogeneous porous media. Vadose Zone J 3:837–847

Eccles JK, Pratson L, Newell RG, Jackson RB (2009) Physical and economic potential of geological CO_2 storage in saline aquifers. Environ Sci Technol 43:1962–1969

Eigestad GT, Dahle HK, Hellevang B, Riis F, Johansen WT, Øian E (2009) Geological modeling and simulation of CO_2 injection in the Johansen formation. Comput Geosci 13:435–450

Ennis-King J, Preston I, Paterson L (2005) Onset of convection in anisotropic porous media subject to a rapid change in boundary conditions. Phys Fluids 17:084107

Esposito A, Benson SM (2010) Optimization of remediation of possible leakage from geologic CO_2 storage reservoirs into groundwater aquifers. Soc Pet Eng SPE 133604:1–12

He J, Fang S, Hou F, Yan R, Zhao Z, Yao J, Tang X, Wu G (2013) Vertical zonation of weathered crust ancient karst and reservoir evaluation and prediction: a case study of M55-M51 sub-members of Majiagou Formation in gas fields, central Ordos Basin, NW China. Pet Explor Dev 40:572–581

Houghton JT, Meira-Filho LG, Callander BA, Harris N, Kattenburg A, Maskell Ke (1996) Climate change 1995: the science of climate change—contribution of working group I to the second assessment report of the Intergovernmental Panel on Climate Change. Cambridge University Press, Cambridge

IPCC (2005) IPCC special report on carbon dioxide capture and storage. Cambridge University Press, Cambridge

Jahangiri HR, Zhang D (2011) Effect of spatial heterogeneity on plume distribution and dilution during CO_2 sequestration. In J Greenhouse Gas Control 5:281–293

Jiao Z, Surdam RC, Zhou L, Stauffer PH, Luo T (2011) A feasibility study of geological CO_2 sequestration in the Ordos Basin, China. Energy Procedia 4:5982–5989

Jung NH, Han WS, Watson ZT, Graham JP, Kim KY (2014) Fault-controlled CO_2 leakage from natural reservoirs in the Colorado Plateau, east-central Utah. Earth Planet Sci Lett 403:358–367

Kopp A, Class H, Helmig R (2009) Investigations on CO_2 storage capacity in saline aquifers, part 2: estimation of storage capacity coefficients. Int J Greenhouse Gas Control 3:277–287

Law DHS, Bachu S (1996) Hydrogeological and numerical analysis of CO_2 disposal in deep aquifers in the Alberta sedimentary basin. Energy Convers Manag 37:1167–1174

Ledley TS, Sundquist ET, Schwartz SE, Hall DK, Fellows JD, Killeen TL (1999) Climate change and greenhouse gases. EOS, Trans Am Geophys Union 80:453–458

Li R, Li Y (2008) Tectonic evolution of the western margin of the Ordos Basin (central China). Russ Geol Geophys 49:23–27

Li X, Liu Y, Bai B, Fang Z (2006) Ranking and screening of CO_2 saline aquifer storage zones in China. Chin J Rock Mech Eng 25:963–968

Li Q, Liu G, Liu X, Li X (2013) Application of a health, safety, and environmental screening and ranking framework to the Shenhua CCS project. Int J Greenhouse Gas Control 17:504–514

Liu M, Liu Z, Liu J, Zhu W, Huang Y, Yao X (2014) Coupling relationship between sandstone reservoir densification and hydrocarbon accumulation: a case from the Yanchang Formation of the Xifeng and Ansai areas, Ordos Basin. Pet Explor Dev 41:185–192

Lumley D (2010) 4D seismic monitoring of CO_2 sequestration. Lead Edge 29:150–155

Martens S, Liebscher A, Möller F, Würdemann H, Schilling F, Kühn M (2011) Progress report on the first European on-shore CO_2 storage site at Ketzin (Germany): second year of injection. Energy Procedia 4:3246–3253

McPherson BJOL, Cole BS (2000) Multiphase CO_2 flow, transport and sequestration in the Powder River Basin, Wyoming, USA. J Geochem Explor 69:65–69

Michael K, Golab A, Shulakova V, Ennis-King J, Allinson G, Sharma S, Aiken T (2010) Geological storage of CO_2 in saline aquifers: a review of the experience from existing storage operations. Int J Greenhouse Gas Control 4:659–667

Mualem Y (1976) A new model for predicting the hydraulic conductivity of unsaturated porous media. Water Resour Res 12:513–522

Oladyshkin S, Class H, Helmig R, Nowak W (2011) A concept for data-driven uncertainty quantification and its application to carbon dioxide storage in geological formations. Adv Water Resour 34:1508–1518

Oldenburg CM (2008) Screening and ranking framework for geologic CO_2 storage site selection on the basis of health, safety, and environmental risk. Environ Geol 54:1687–1694

Preston C, Monea M, Jazrawi W, Brown K, Whittaker S, White D, Law D, Chalaturnyk R, Rostron B (2005) IEA GHG Weyburn CO_2 monitoring and storage project. Fuel Process Technol 86:1547–1568

Pruess K (2005) ECO2N: a TOUGH2 fluid property module for mixtures of water, NaCl, and CO_2. Lawrence Berkeley National Laboratory Berkeley, Berkeley, CA

Pruess K (2008) Leakage of CO_2 from geologic storage: role of secondary accumulation at shallow depth. Int J Greenhouse Gas Control 2:37–46

Qiu X, Liu C, Mao G, Deng Y, Wang F, Wang J (2014) Late Triassic tuff intervals in the Ordos basin, Central China: their depositional, petrographic, geochemical characteristics and regional implications. J Asian Earth Sci 80:148–160

Ran X, Fu J, Wei X, Ren J, Sun L, Bao H (2012) Evolution of the Ordovician top boundary and its relationship to reservoirs' development, Ordos Basin. Pet Explor Dev 39:165–172

Ren XK, Cui YJ, Bu XP, Tan YJ, Zhang JQ (2010) Analysis of the potential of CO_2 geological storage in the Ordos basin. Energy China 32:29–32

Saripalli P, McGrail P (2002) Semi-analytical approaches to modeling deep well injection of CO_2 for geological sequestration. Energy Convers Manag 43:185–198

Span R, Wagner W (1996) A new equation of state for carbon dioxide covering the fluid region from the triple-point temperature to 1100 K at pressures up to 800 MPa. J Phys Chem Ref Data 25:1509–1596

Sun Y, Su RN (2012) Analysis on characteristics of temperature variation in Ordos in recent 51 years. Meteorol J Inn Mong 5:16–18

US DOE (2007) Carbon sequestration ATLAS of the United States and Canada Office of Fossil Energy, National Energy Technology Laboratory, Morgantown, WV, 90 pp

Van der Zwaan B, Gerlagh R (2009) Economics of geological CO_2 storage and leakage. Clim Chang 93:285–309

Van Genuchten MT (1980) A closed-form equation for predicting the hydraulic conductivity of unsaturated soils. Soil Sci Soc Am J 44:892–898

Vilarrasa V, Bolster D, Dentz M, Olivella S, Carrera J (2010) Effects of CO_2 compressibility on CO_2 storage in deep saline aquifers. Transp Porous Media 85:619–639

Watson FE, Mathias SA, Daniels SE, Jones RR, Davies RJ, Hedley BJ, van Hunen J (2014) Dynamic modelling of a UK North Sea saline formation for CO_2 sequestration. Pet Geosci 20:169–185

Wu X (2013) Carbon dioxide capture and geological storage: the first massive exploration. China Science Press, Beijing

Wu XZ (2014) Shenhua Group's carbon capture and storage (CCS) demonstration. Mining Rep 150:81–84

Xie J, Zhang K, Hu L, Wang Y, Chen M (2015) Understanding of the carbon dioxide sequestration in low-permeability saline aquifers in the Ordos Basin with numerical simulations. Greenhouse Gases Sci Technol 5:1–19

Yang H, Deng X (2013) Deposition of Yanchang Formation deep-water sandstone under the control of tectonic events in the Ordos Basin. Pet Explor Dev 40:549–557

Yang H, Fu J, He H, Liu X, Zhang Z, Deng X (2012) Formation and distribution of large low-permeability lithologic oil regions in Huaqing, Ordos Basin. Pet Explor Dev 39:683–691

Yang R, He Z, Qiu G, Jin Z, Sun D, Jin X (2014) A Late Triassic gravity flow depositional system in the southern Ordos Basin. Pet Explor Dev 41:724–733

Zhang W, Li Y, Xu T, Cheng H, Zheng Y, Xiong P (2009) Long-term variations of CO_2 trapped in different mechanisms in deep saline formations: a case study of the Songliao Basin, China. Int J Greenhouse Gas Control 3:161–180

Zhao R, Cheng J, Zhang K (2012) CO_2 plume evolution and pressure buildup of large-scale CO_2 injection into saline aquifers in Sanzhao Depression, Songliao Basin, China. Transp Porous Media 95:407–424

Zhou Q, Birkholzer JT, Tsang CF, Rutqvist J (2008) A method for quick assessment of CO_2 storage capacity in closed and semi-closed saline formations. Int J Greenhouse Gas Control 2:626–639